ASME Journal of Engineering for Gas Turbines and Power
Online journal at:
https://asmedigitalcollection.asme.org/gasturbinespower

Numerical Investigation of Premixed and Non-Premixed Hydrogen Flames Using Large-Eddy Simulations and Flamelet Models

Antonio Masucci[1]
Department of Mechanical, Chemical and Materials Engineering,
Università degli Studi di Cagliari,
Via Marengo 2,
Cagliari 09123, Italy
e-mail: antonio.masucci@unica.it

Tiziano Ghisu
Department of Mechanical, Chemical and Materials Engineering,
Università degli Studi di Cagliari,
Via Marengo 2,
Cagliari 09123, Italy
e-mail: tiziano.ghisu@unica.it

Andrea Giusti
Department of Mechanical Engineering,
Imperial College London,
South Kensington Campus,
London SW7 2AZ, UK
e-mail: a.giusti@imperial.ac.uk

A numerical investigation of premixed and nonpremixed hydrogen flames is performed with the main aim of assessing the capability of large-eddy simulations (LES) and flamelet models to predict the main characteristics of the reactive field. Two different burners are investigated: (i) a premixed bluff body burner fueled with a lean hydrogen–air mixture ($\phi = 0.4$) and (ii) a nonpremixed dual-swirl coaxial injector for which experiments show both anchored and lifted flames for the same global equivalence ratio ($\phi_g = 0.45$). Simulations of the premixed burner are performed using the Flamelet Generated Manifold (FGM) approach, whereas the two types of flames realized in the nonpremixed burner are studied using the Steady Diffusion Flamelet (SDM) and the Flamelet Generated Manifold. Numerical results are compared with the available experimental data for flow and flame characterization. As far as the velocity field is concerned, the investigated flamelet models have demonstrated capability to properly predict the location and magnitude of the velocity peaks and the shape of the inner recirculation zone (IRZ) in both the premixed and nonpremixed cases. Moreover, the computational framework used in this study has demonstrated good accuracy in the prediction of the dynamic behavior of the flow. Regarding the structure of the flame, the models have shown a good capability to predict both the shape of the flame and the location of regions of high-intensity heat release rate (HRR). The present investigation offers a comprehensive assessment of large-eddy simulations and flamelet methods in the prediction of the behavior of two archetypes of hydrogen flames of industrial interest. The assessment shown here can provide support for the choice of methods to study cases with increased level of complexity. [DOI: 10.1115/1.4069451]

Keywords: turbulent combustion, large eddy simulation, hydrogen combustion, bluff-body, swirling flames, premixed combustion, non-premixed combustion, flamelet

1 Introduction

Hydrogen is one of the most promising fuels to decarbonize the energy and transportation sectors, due to the zero-carbon emissions produced by its direct combustion. However, hydrogen combustion remains very challenging due to the very different physical and chemical properties of this fuel compared to standard fuels used in propulsion and power generation. For instance, compared to widely used hydrocarbons, hydrogen is characterized by very high molecular diffusion, low activation energy, and fast laminar burning velocity [1–3], which make not straightforward the use of hydrogen in combustors originally designed to operate with hydrocarbon fuels. In addition, the high reactivity of hydrogen may result in high NOx emissions and risk of flashback if mitigation measures are not adopted. Therefore, to enable an extensive use of hydrogen, new combustion technologies must be developed together with an improved understanding of the combustion characteristics of hydrogen in flames of practical interest. In the context of transition to a zero-carbon economy, it is also important to remark that production and storage of hydrogen still have their own challenges, which must be addressed together with the development of combustion technologies [4]. Lean premixed flames, where the temperature of the reacting region can be controlled through the composition of the mixture, are still considered a reference technology for the limitation of emissions, especially NO_x. However, when hydrogen is used, the risk of flashback can greatly increase [5]. Therefore, new technologies have been proposed such as microjets, which limit the risk of flashback by injecting hydrogen through an array of nonpremixed jets. This nonpremixed configuration consists of injecting hydrogen through an array of high-momentum jets of submillimeter radius [6]. The objective of

Turbo Expo: Turbomachinery Technical Conference & Exposition (GT2025), June 16–20, 2025. GT2025.
[1]Corresponding author.
Manuscript received June 27, 2025; final manuscript received July 21, 2025; published online September 24, 2025. Editor: Jerzy T. Sawicki.

micromixing is to separate fuel and oxidizer prior to injection, therefore avoiding flashback, and at the same time enabling a quick mixing in the vicinity of the injection plate to ensure a quick transition to a premixed regime [7]. Therefore, to develop reliable and safe combustion systems, it remains necessary to develop fundamental understanding of hydrogen flame behavior in the two extreme configurations of fully premixed and nonpremixed combustion. Premixed flames occur when fuel and oxidizer are thoroughly mixed before entering the combustion chamber. The advantages of premixed flames include efficient and uniform combustion, reduced emissions, and greater control over combustion processes, making them ideal for applications requiring low (or controlled) release of pollutants. The main drawbacks of premixed flames include susceptibility to flame instability, limited operating range due to flammability limits, and potential for flashback or combustion oscillations under certain conditions [8], making them more difficult to control than nonpremixed flames. Also, some pollutants are more prone to appear in premixed conditions than nonpremixed ones. On the other hand, nonpremixed flames allow greater flexibility in adjusting fuel-oxidizer ratios for specific combustion requirements, wider operating ranges, and reduced risk of flashback, offering versatility in various combustion applications. However, nonpremixed flames present potential for incomplete combustion leading to higher emissions of pollutants, increased sensitivity to variations in flow conditions, and the need for complex control mechanisms to maintain flame stability [9]. Different types of geometries can be used to help in the stabilization of the flame and to reduce the emission of NO_x such as bluff bodies and swirling flows [10]. In particular, it has been noticed that the latter produce an IRZ (inner recirculation zone) of the hot gases that enhances flame stabilization and serves as a source of energy for the incoming reactants. The interaction between swirling flows and a reacting field determines the flame shape and location. It has been observed that changes in the geometry and flow characteristics (e.g., swirl number) could lead to different anchoring points of the flame. An example is provided by Marragou et al., who report an analysis of the transition from an anchored to a lifted flame [11]. This phenomenon is relevant because a lifted flame operates mainly in a partially premixed regime, leading to a substantial reduction in NO_x. To gain further understanding over the combustion process of hydrogen for flames of practical interest and to validate models used for the prediction of the flame behavior, three different test cases have been recently released by the International Workshop on Measurement and Computation of Turbulent Flames [12]. For all these test cases, measurements on pure hydrogen premixed and nonpremixed flames are provided. Numerical simulations nowadays play crucial role in the design of combustion units, e.g., to downselect burner configurations or conduct optimization analysis. In the context of flames characterized by a high level of unsteadiness and anisotropity (e.g., vortex breakdown phenomena in swirling flows), large-eddy simulations (LES) offer the possibility to provide an accurate prediction of the mixing field. The presence of a reacting field also introduces scales related to chemistry. When turbulence–chemistry interactions are important (low *Da* flames), a time-resolved description of the flame structure with detailed chemistry is needed for a reliable characterization of the flame behavior [13]. If the chemical time scales are small compared to the time scales associated with turbulence, a flamelet description of the flame structure has been proven to provide accurate predictions. Moreover, if the flame is working in a flamelet regime, complex detailed combustion mechanisms can be used to build a flamelet library without increasing the computational cost. Although numerical methods have been extensively assessed and validated for hydrocarbon fuels, when it comes to hydrogen, which is characterized by a significantly different behavior compared to hydrocarbon fuels, such detailed validation of the numerical tools has not been performed yet. Aniello et al. [14] have investigated the nonpremixed flame studied at the Institut de-Mécanique des Fluides de-Toulouse using the dynamic thickened flame model showing that the thickened flame model is able predict the behavior of the two types of flames thereby investigated. The same test rig was investigated by Ballotti et al. [15] where a dynamic thickening strategy for high-fidelity computational fluid dynamics was developed for the analysis of multiregime combustion. Some works using flamelet models are also available on the premixed flame studied at the Norwegian University of Science and Technology (NTNU) [16,17], even though the operating conditions used in these works are different and there are also small differences in the geometry used by the authors. In the latter, different CH_4/H_2–air mixtures have been investigated with LES, including the use of various models for the reaction rate source term. The same burner was also investigated in Refs. [18–20] using a thickened flame model to study the phenomena associated with ignition. With the overall aim of further assessing the ability of established models to predict the characteristics of hydrogen flames of industrial interest, the objectives of the present work are to (i) investigate the capability of flamelet models to predict the flame structure and the behavior of the flow of premixed and nonpremixed hydrogen flames; (ii) assess the capability of flamelet models to provide a reliable prediction of the dynamic behavior of the flame, including liftoff. The first objective is addressed by comparing the experimental measurements of the mean axial and radial velocities against the corresponding time-averaged results obtained by the LES. In addition, available experimental data on OH-Chemiluminescence and OH-PLIF are respectively compared with the time averaged results of heat release rate (HRR) and OH mass fraction in order to study the flame structure. The second objective is addressed by comparing the available measurement on the dynamic behavior of the flow such as the root mean square (RMS) of the axial and radial velocity fluctuations against LES results. A flame that exhibits liftoff has also been selected to assess the capability of the selected models to predict lifted flames. The paper is structured as follows: First, the configuration and investigated cases are described. Then, the numerical methods and computational setup are presented. This is followed by the presentation of results and their discussion. A summary of the work and main conclusions close the paper.

2 Configuration and Investigated Cases

Two different test cases are investigated in this work. The first case, which will be referred to as "NTNU" case, is a bluff-body premixed flame. The second case, which will be referred to as "HYdrogen LOw NOx (HYLON)" case, is a nonpremixed swirled flame. These two test cases allow us to cover the most common flame and flow configurations, therefore providing a comprehensive assessment of the models investigated here. The two geometries are presented in detail in Secs. 2.1 and 2.2.

2.1 Norwegian University of Science and Technology Case. The premixed flame configuration studied at the NTNU consists in a bluff-body stabilized burner. A schematic of the geometry is shown in Fig. 1. The conical bluff body has a diameter $d_b = 13$ mm and half-cone angle $\alpha = 45$ deg. The hydrogen–air mixture is injected through an annular duct surrounding the bluff-body holder. The external diameter of the inlet duct is $d_i = 19$ mm, whereas the bluff-body holder has a diameter of 5 mm. The burner downstream of the bluff body operates with no confinement. Therefore, the flame develops in a free environment at ambient pressure and temperature.

The bluff body's holder is centered by a set of three transversal cylinders (of diameter 2 mm each) that are placed at a distance of 65 mm upstream of the bluff-body top surface. The location of these cylinders is sufficiently far upstream not to affect the flame dynamics [21–23]. Regarding the operating conditions, the hydrogen–air mixture is injected at room temperature, $T_{amb} = 25\,^{\circ}$C. The mass flowrate of hydrogen and air are equal to $\dot{m}_{H_2} = 2.92 \times 10^{-5}$ kg/s and $\dot{m}_{air} = 2.258 \times 10^{-3}$ kg/s, respectively. The equivalence ratio is kept constant at $\phi = 0.4$; the laminar flame properties at this equivalence ratio are reported in Table 1.

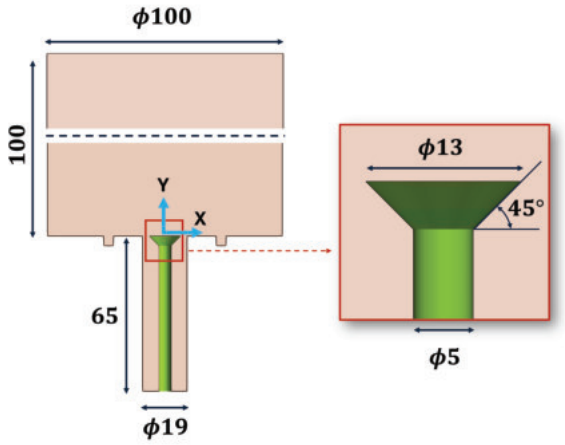

Fig. 1 Schematic of the NTNU premixed hydrogen burner: three-dimensional (3D) view of the burner assemble (left) and vertical cross section passing through the bluff-body axis (right). All dimensions are reported in mm.

Table 1 Laminar flame properties at ϕ=0.4

ϕ	T_{ad} (K)	s_l (m/s)	δ_l (m)	τ_f (s)
0.4	1434	0.21	6.5×10^{-4}	0.0031

From left to right: adiabatic flame temperature, laminar flame speed, laminar flame thickness, and chemical time scale.

Given that LHV = 120 MJ/kg, the hydrogen flowrate supplied to the rig results in a thermal power of the burner equal to $P_{th} = 3.5$ kW.

2.2 HYdrogen LOw NOx Case. The nonpremixed flame studied in this work is the HYLON burner (HYdrogen LOw NOx) dual swirl injector investigated at the Insitut de-Mécanique des Fluides de-Toulouse. A schematic of the configuration is shown in Figs. 2 and 3.

The burner is characterized by two swirling coaxial ducts for the separate injection of hydrogen and air with dimension $d_{air} = 18$ mm and $d_{H_2} = 4$ mm, respectively. The combustion chamber has the

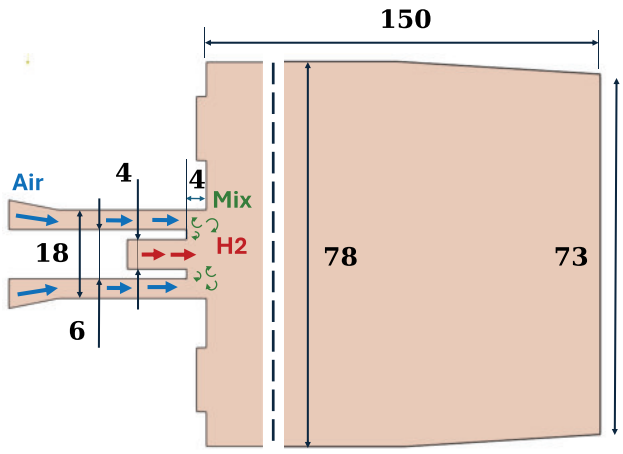

Fig. 2 Schematic of the HYLON nonpremixed hydrogen burner: 3D view of the burner confinement (left), and 3D view of the injector (right). Hydrogen and air are injected through two separate ducts (yellow for air and red for hydrogen). Both streams are swirled and before the combustion chamber there is a zone to enhance the mixing between the two streams. (Color version online.)

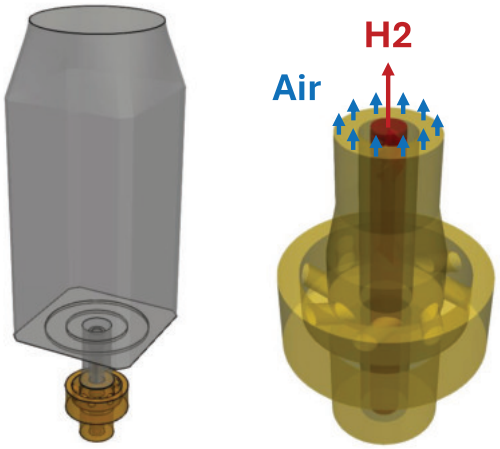

Fig. 3 Cross section of the HYLON burner passing through the axis of the injector (all dimensions are in mm)

Table 2 HYLON operating conditions for the two flames investigated in this work

Flame	$\dot{m}_{air}$ (kg/s)	$\dot{m}_{H_2}$ (kg/s)	T_{air} (K)	T_{H_2} (K)	P_{th} (kW)	p (Pa)
A	2.41×10^{-3}	3.2×10^{-5}	298	298	3.89	101,325
L	6.03×10^{-3}	8.0×10^{-5}	298	298	9.73	101,325

following dimensions: side $h_c = 78$ mm, length $L_c = 150$ mm and outflow diameter $d_o = 73$ mm. A gap of $z_i = 4$ mm between the exit of the hydrogen nozzle and the entry of the combustion chamber enhances the mixing between the two streams. Two different operating conditions are investigated in this work: Flame A, which is attached to the hydrogen nozzle, and Flame L which is lifted above the fuel injector. The flow and fuel quantities for these operating conditions are reported in Table 2.

3 Methods

3.1 Large-Eddy Simulations-Flamelet Model. Numerical simulations are performed using the LES approach coupled with tabulated flamelets. Following the flamelet approach, it is assumed that the turbulence does not affect the flame structure [24], which can be represented by precomputed laminar flames. Progress variable and mixture fraction are used to identify the local burning state and composition of the mixture. The effect of turbulence on the flame characteristics is modeled with a presumed-pdf approach, computed from the filtered values of the progress variable and mixture fraction and their subgrid scale variances. Pretabulated flamelet libraries are built using a Beta Probability Density Function (β – PDF). In this work, two different flamelet models are used and evaluated:

- The *Steady Diffusion Flamelet* (SDM), where the control variables are the filtered mixture fraction, $\tilde{Z}$, its sub-grid scale variance, $\widetilde{Z''^2}$, and the stoichiometric scalar dissipation rate $\tilde{\chi}_{st}$ (i.e., the scalar dissipation rate at $Z = Z_{st}$). The stoichiometric scalar dissipation rate is computed from the mixing field solution with the following algebraic closure:

$$\tilde{\chi}_{st} = C_\chi \frac{\mu_{sgs} + \mu}{\rho \sigma_t} |\nabla \tilde{Z}|^2 \tag{1}$$

where C_x is a constant with a default value of 2 [25], μ and μ_{sgs} are respectively the molecular and the subgrid scale viscosity, ρ is the density, σ_t is a constant turbulent Prandtl/Schmidt number, and $\tilde{Z}$ corresponds to the filtered mixture fraction. The stoichiometric scalar dissipation rate is included in the

tabulation using a delta-function PDF. Therefore, the filtered value of a generic variable, $\tilde{\alpha}$, can be obtained as

$$\tilde{\alpha}(\tilde{Z}, \widetilde{Z''^2}, \tilde{\chi}_{st}) = \int\int \alpha(Z, \chi_{st}) P_Z(\tilde{Z}, \widetilde{Z''^2}) P_\chi(\chi_{st})\, dZ\, d\chi_{st} \quad (2)$$

- The *Flamelet Generated Manifold* (FGM), where the control variables used for the flamelet tabulation are the filtered mixture fraction, $\tilde{Z}$, its subgrid scale variance, $\widetilde{Z''^2}$, the filtered progress variable, $\tilde{c}$, and its subgrid scale variance, $\widetilde{c''^2}$. In the FGM approach, the filtered value of a generic variable, $\tilde{\alpha}$, is pre-tabulated as

$$\tilde{\alpha}(\tilde{Z}, \widetilde{Z''^2}, \tilde{c}, \widetilde{c''^2}) = \int\int \alpha(Z, c) P_Z(\tilde{Z}, \widetilde{Z''^2}) P_c(\tilde{c}, \widetilde{c''^2})\, dZ\, dc \quad (3)$$

The mean reaction rate in the filtered progress variable transport equation is modeled as proposed by Zimont [26].

Both these flamelet models are implemented by default in ANSYS FLUENT R23.1, which is the software used for the present investigation. As far as the combustion mechanism is concerned, the reduced GRI MECH 3.0 with 10 species and 29 reactions was used in both simulations [27]. Since experimental measurements of OH* are available for the HYLON burner, the OH* reactions have been added to the combustion mechanism following Ref. [28]. The look-up tables were built by integrating the results obtained from one-dimensional laminar flame simulations using ANSYS FLUENT.

3.2 Numerical Setup. In the following, the computational domain and numerical setup of the two test cases are discussed in detail. The computational domains and mesh were built using ICEM CFD R19.

3.2.1 Norwegian University of Science and Technology Case. The computational domain starts immediately after the set of three cylinders that were placed 65 mm upstream of the bluff-body plane. The open atmosphere above the bluff-body is modeled as a cylinder with a diameter $d = 100$ mm and height $h = 100$ mm. This is schematically shown in Fig. 4.

The domain was discretized with a grid of 8 million hexahedral cells. The mesh in the boundary layers was built in order to keep the y^+ value at all walls below 1.0. Table 3 reports the boundary conditions used in the computations. The respective boundaries are indicated in Fig. 5. Figure 5 also reports the different locations that were used to compare numerical simulations with experimental data. Green lines correspond to locations that were used for both cold and reactive flow simulations, while blue and red lines indicate locations where only cold or reactive flow, respectively, were assessed against experiments. A mass flowrate of $\dot{m} = 0.00229$ kg/s was imposed at the mixture stream inlet, as a result of the sum between $\dot{m}_{air}$ and $\dot{m}_{H_2}$ (see Table 1). The mixture fraction value imposed at the mixture inlet, $Z = 0.0125$, was calculated from the

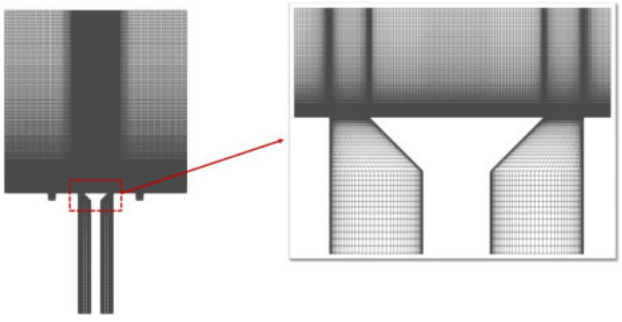

Fig. 4 NTNU computational domain. A structured mesh was used with a refinement of the grid near the wall in order solve the boundary layer.

Table 3 Boundary conditions used for the investigation of the NTNU case

NTNU boundary conditions	
H2 + air stream	Mass flow inlet
Bluff body	No-slip wall
Inlet duct	No-slip wall
Plate	No-slip wall
External surface	Pressure outlet
Outlet	Pressure outlet

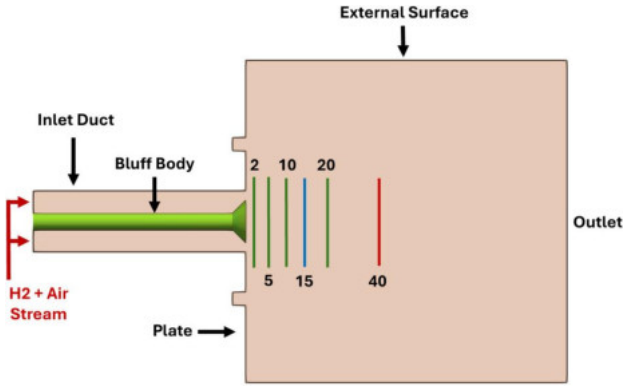

Fig. 5 Boundary patches and locations at which comparison between experimental data and computations is performed for the NTNU test case. The solid lines upstream of the bluff body indicate the axial locations where LES results were extracted and compared with the experimental data.

experimental equivalence ratio ($\phi = 0.4$). Both cold and reactive flow simulations were performed. A time-step of 1×10^{-7} s was chosen to keep the Courant number below unity. The FGM model was selected for the reactive flow. The look-up table was built using premixed freely propagating one-dimensional laminar flames.

To assess the capability of the simulations to capture the flow structures, time-averaged and RMS of axial and radial velocity components were compared with the experimental data. The capability of the model to predict the flame structure was assessed through comparisons with experimental data on OH-PLIF and OH*Chemiluminescence. These two quantities were compared with the time-averaged OH mass fraction and the time-averaged HRR, respectively. The HRR was calculated as proposed by Ref. [17]:

$$\mathrm{HRR} = \rho\ \mathrm{PFR}\ \mathrm{LHV}_{H_2} \tilde{Z} \quad (4)$$

where ρ is the density of the gas, *PFR* is the Product Formation Rate $(1/s)$, LHV_{H_2} is the lower heating value of hydrogen, and $\tilde{Z}$ is the filtered mixture fraction.

The suitability of the mesh for LES simulations was verified by checking whether at least 80% of the turbulent kinetic energy was resolved [29]. The resolved spectrum of turbulent kinetic energy was calculated as follows using the Cèlik criterium [30]:

$$\mathrm{LES}_{IQ} = \frac{1}{1 + 0.05\left(\frac{\nu + \nu_{SGS}}{\nu}\right)^{0.53}} \quad (5)$$

where ν is the kinematic viscosity and ν_{SGS} is the kinematic subgrid viscosity. Results for the reactive flow simulation are shown in A, which demonstrate that more than the 80% of the kinetic energy is solved throughout the computational domain.

3.2.2 HYdrogen LOw NOx Case. The computational domain for the HYLON test case comprises the burner geometry downstream of the hydrogen and air injection location. This domain was discretized with a structured mesh of 5 million cells, shown in Fig. 6.

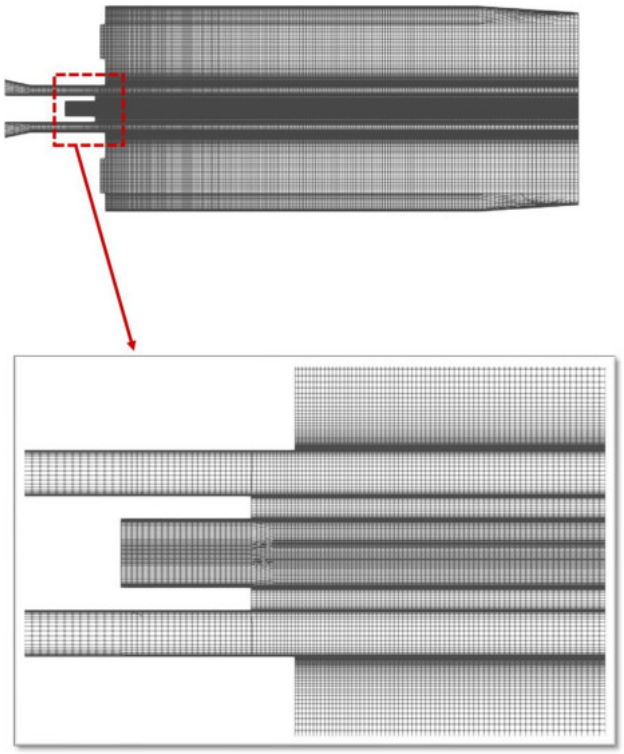

Fig. 6 Geometry decomposition for the HYLON case and meshing strategy

Swirler ducts were not included in the computational domain. The velocity profiles assigned at the air and fuel inlets were computed by performing a preliminary Reynolds-Averaged Navier–Stokes (RANS) simulation of the injector only, discretized with an unstructured mesh of tetrahedral cells (see also Fig. 7). The preliminary RANS simulation of the injector was carried out with the k–ω SST turbulence model. Profiles of x, y, and z components of the velocity and of turbulent kinetic energy k and specific dissipation rate ω were then extracted and assigned as inlet conditions for the burner.

For the simulation of this burner, the SDM model was used for Flame A, whereas the FGM model was used for Flame L. This choice was made because, as explained by Ref. [11], the lifted flame evolves mainly in the partially premixed regime where the FGM model performs better than an approach for nonpremixed flames only. Large-eddy simulations were carried out using a time-step of

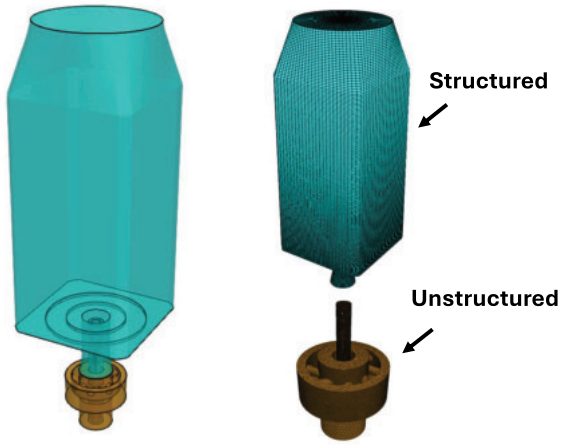

Fig. 7 HYLON computational domain

Table 4 HYLON boundary conditions

HYLON boundary conditions	
H2 stream	Velocity inlet (profile)
Air stream	Velocity inlet (profile)
Combustion chamber	No-slip wall
Inlet duct	No-slip wall
Plate	No-slip wall
Outlet	Pressure outlet

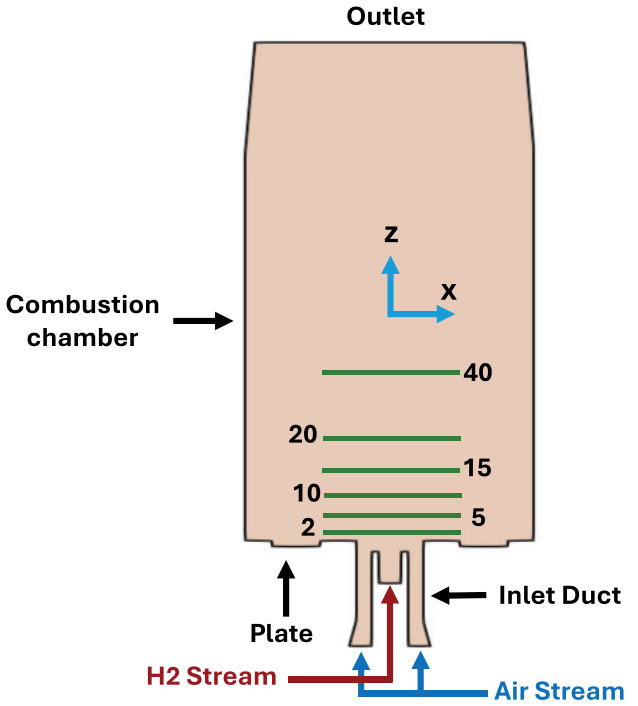

Fig. 8 Boundary patches and locations at which comparison between experimental data and computations is performed for the HYLON test case

1×10^{-7} s. Table 4 reports the boundary conditions. The corresponding boundaries are labeled in Fig. 8.

Comparison with experiments was performed in terms of time-averaged and RMS values of axial and radial components of the velocity. Figure 8 shows the locations where experimental data were extracted for both the cold and reactive flow simulations. Moreover, measurements of OH* chemiluminescence are available to study the flame structure. This set of data was compared with the time-averaged OH* mass fraction obtained from LES. An analysis of the resolved and modeled turbulent kinetic energy in the reactive flow simulation is reported in A. This analysis demonstrates that more than 80% of the kinetic energy was solved throughout the computational domain.

4 Results and Discussion

4.1 Norwegian University of Science and Technology Case. Figures 9 and 10 show the comparisons between the time-averaged and RMS values of the axial and radial velocity components at different axial positions. Simulations are in good agreement with the experiments. In particular, simulations are able to predict the peaks of the axial and radial velocity components as well as the RMS of their fluctuations. Also, by comparing the axial velocity of the cold flow and reactive flow cases (see Fig. 10), it is possible to note the increase in the extent of the IRZ. Concerning the behavior of velocity fluctuations, the LES is able to predict the

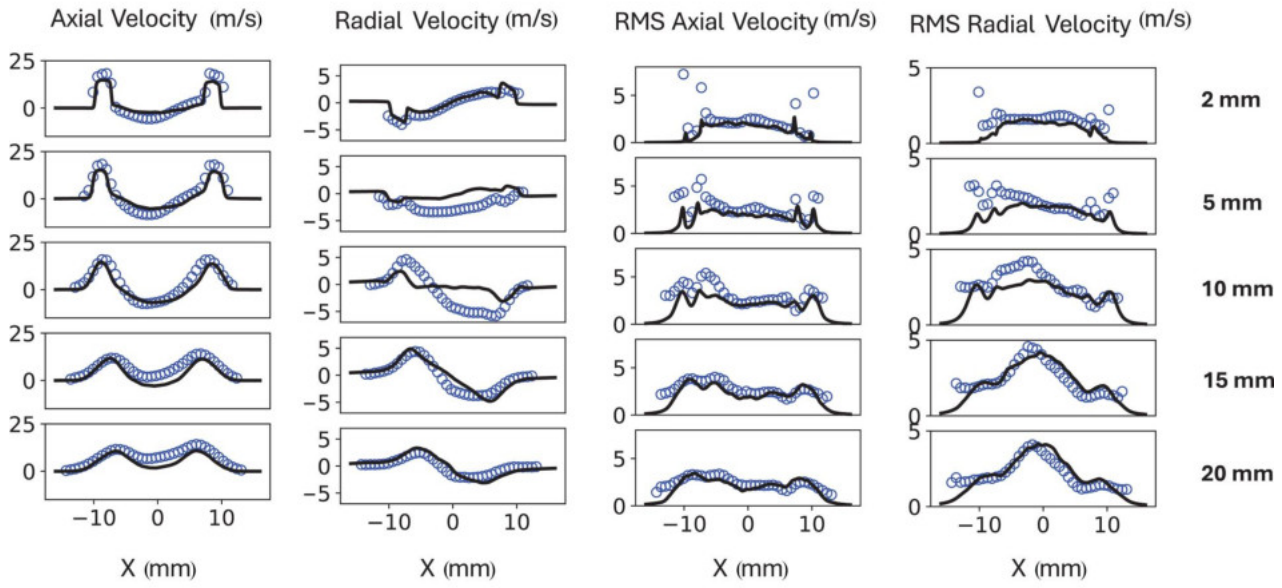

Fig. 9 NTNU cold flow simulation (LES:▬, Exp: o)

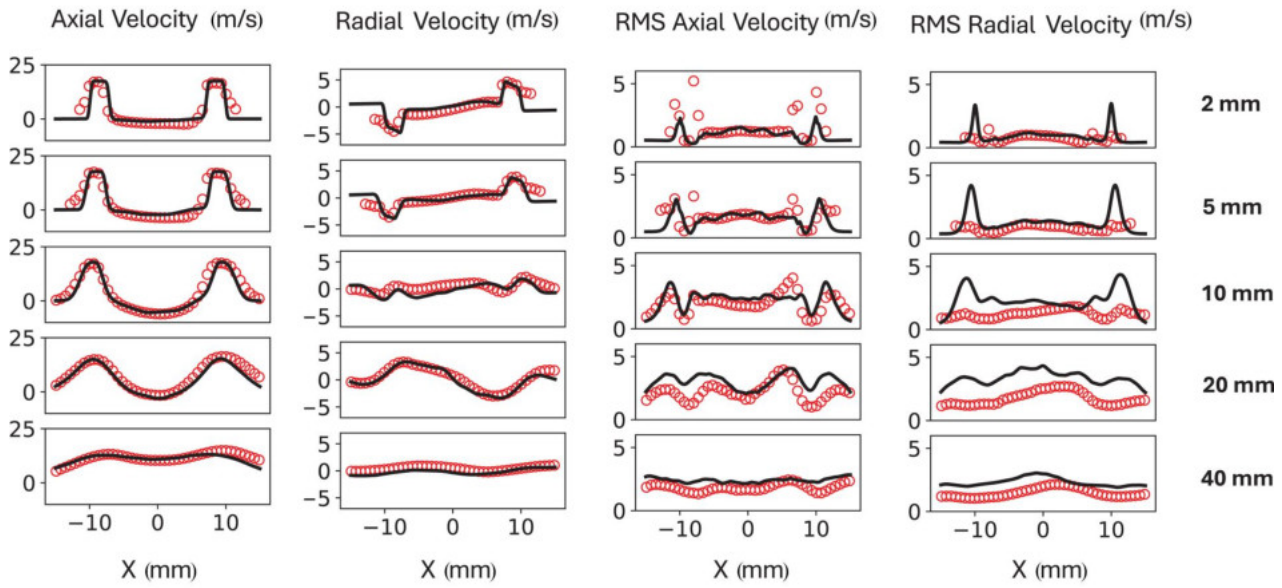

Fig. 10 NTNU reactive flow simulation (LES:▬, Exp: o)

evolution of the RMS of both the axial and radial velocities in the cold flow. However, in the reactive flow, the RMS of the radial velocity in the shear layer is overpredicted. The overprediction is also significant in the central region at a height of 20 mm. The flow fluctuations in the reacting simulations are the result of the coupling between the flow dynamics and the changes in density and composition due to chemical reactions. Accurately reproducing velocity fluctuations in reacting flows is challenging. These results demonstrate that the modeling framework investigated here is able to predict the time-averaged behavior. However, refinements may be necessary to further improve the prediction of fluctuations. Figure 11 shows the time-average velocity and RMS of velocity fluctuations in a cross section passing through the axis of the bluff-body. Numerical results are compared with experiments. As already discussed, the time-averaged velocity components are predicted with good accuracy. However, the RMS of the velocity fluctuations tends to be overpredicted both in the shear layers formed at the edges of the bluff-body and annular duct and in the central region of the domain (downstream of the bluff-body). This behavior was also observed in other investigations of bluff-body burners, e.g., Ref. [31].

Regarding the prediction of the flame structure, Fig. 12 shows a comparison between the experimental data of OH* Chemiluminescence and the time-averaged normalized HRR. Figure 12 also shows a comparison between the experimental data for OH-PLIF and the time-averaged OH mass fraction. The flame predicted by the simulation appears thinner than the experimental data. It is worth noting that the FGM model, in its basic formulation implemented in ANSYS FLUENT, does not include the effects of stretch. As discussed by Klarmann et al. [32], the shape of the flame can be more accurately predicted if these effects are included in the construction of the look-up table. Future work will involve implementing more

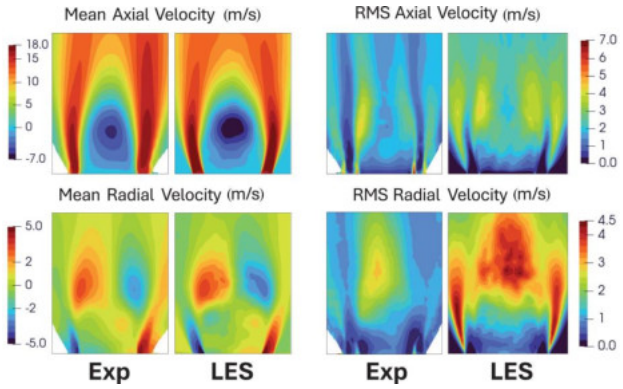

Fig. 11 Contour plot of time averaged and RMS velocities compared to the experimental data

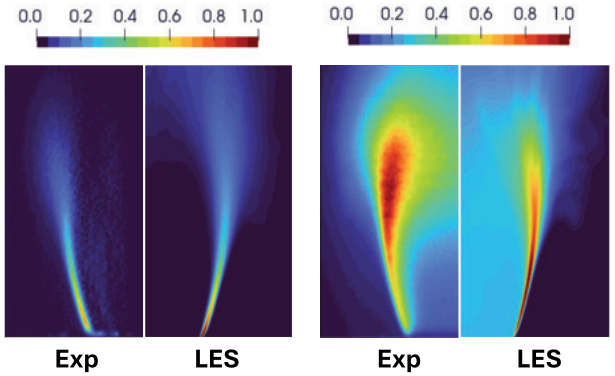

Fig. 12 Left: comparison between OH* Chemiluminescence and time-averaged normalized HRR. Right: comparison between OH PLIF and time averaged OH mass fraction.

accurate models that can account for the effects of stretch and differential diffusion models in order to compare the different approaches.

To further investigate the flame characteristics, the Takeno Index [33] was used to differentiate regions of the flame burning in premixed or nonpremixed mode. Figure 13 shows the instantaneous contour plot of the flame index. A value of +1 indicates premixed combustion, while a value of −1 corresponds to nonpremixed combustion. The combustion regime is fully premixed over the entire flame region and this allows the FGM model to perform at its best since the look-up table was built with premixed flamelets.

4.2 HYdrogen LOw NOx Case. Figures 14 and 15 show the comparison between experimental and numerical velocity components for cold and reactive flows, respectively. Results show that the model is able to predict the axial and radial velocity components in both operating conditions. This means that the shape of the IRZ, as well as the swirled motion, is captured by the model. The RMS of the velocity fluctuations is also well predicted both for the radial and axial components of the velocity. These results suggest that the LES framework used in the present study is able to capture the variations of the velocity flow field between the cold and reactive flow, caused by the thermal expansion of gases.

Table 5 reports a comparison between the experimental values for the averaged temperature of the gases at the outlet of the burner and the time-averaged temperature predicted by LES simulations performed in the present work and the results by Aniello et al. [14]. The LES-flamelet model used in the present work results in overprediction of the temperature for Flame A, whereas for Flame L, the time-averaged temperature is remarkably close to the experimental value.

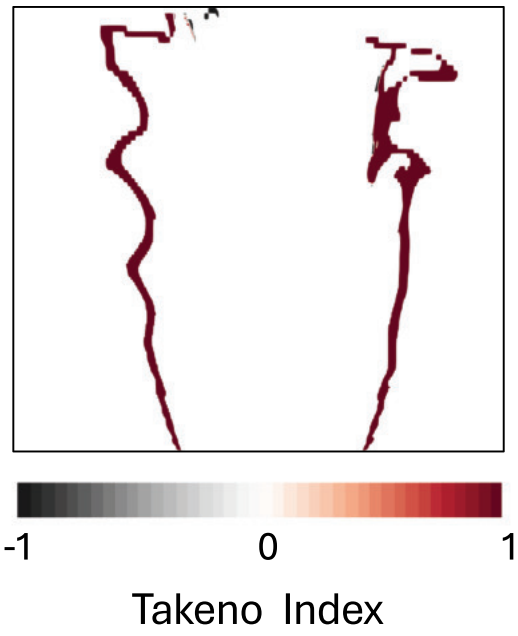

Fig. 13 Instantaneous contour plot of the Takeno Index. A value of +1 indicates premixed combustion, while a value of −1 corresponds to nonpremixed combustion.

To investigate the local presence of multiple flame regimes, the instantaneous contour plot of the Takeno Index is shown in Fig. 16. Unlike the NTNU case, the flame here is characterized by multiple regimes, including both premixed and nonpremixed combustion. This complexity makes the flame characteristics more difficult to predict since the look-up table can only be constructed using either premixed or nonpremixed flamelets. The presence of multiple combustion regimes on the flame front may lead to less accurate predictions due to the use of the table [34]. Moreover, this effect, combined with the limitations of the flamelet models, such as the use of a presumed PDF function and reduced accuracy near walls [35], could result in an overestimation of the temperature, as observed for the attached flame. In this study, enthalpy losses were not considered due to the lack of thermal boundary conditions from the experiments, particularly at the injector lip of the fuel stream. Additionally, radiative heat transfer was neglected.

As far as the flame structure is concerned, Fig. 17 shows a comparison between measurement and numerical predictions of OH*. Overall, the model is able to correctly predict the shape of the visible flame, reproducing the regions of high heat release rate along the shear layer. The absence of OH* in the recirculation region of Flame A is also well predicted. For Flame L, the model is able to predict a thicker flame, the larger area of high heat release rate further downstream of the bluff body, as well as the presence of OH* in the area above the bluff body. Some discrepancies between experiments and numerical simulations are observed in terms of extent of the area with OH* presence and angle between the burner axis and the line where a greater release of OH* is observed, see Fig. 17. Note that the present numerical results are in agreement with the LES-TFUP simulations by Marragou et al. [11], demonstrating that the prediction of the experimental flame angle is a challenge for numerical simulations.

As discussed in Ref. [11], a lifted flame can move upstream only if two conditions are met: (i) a flammable mixture fraction line Z_0, that represent the edge flame propagation line, between the flame and the injector exists and (ii) the mixture fraction Z_0 is located, from the flame to the injector lip, in a zone where the projection of the local velocity u_t along this line is lower than its propagation velocity s_d. The edge flame speed s_d on the Z_0 line is calculated as follows:

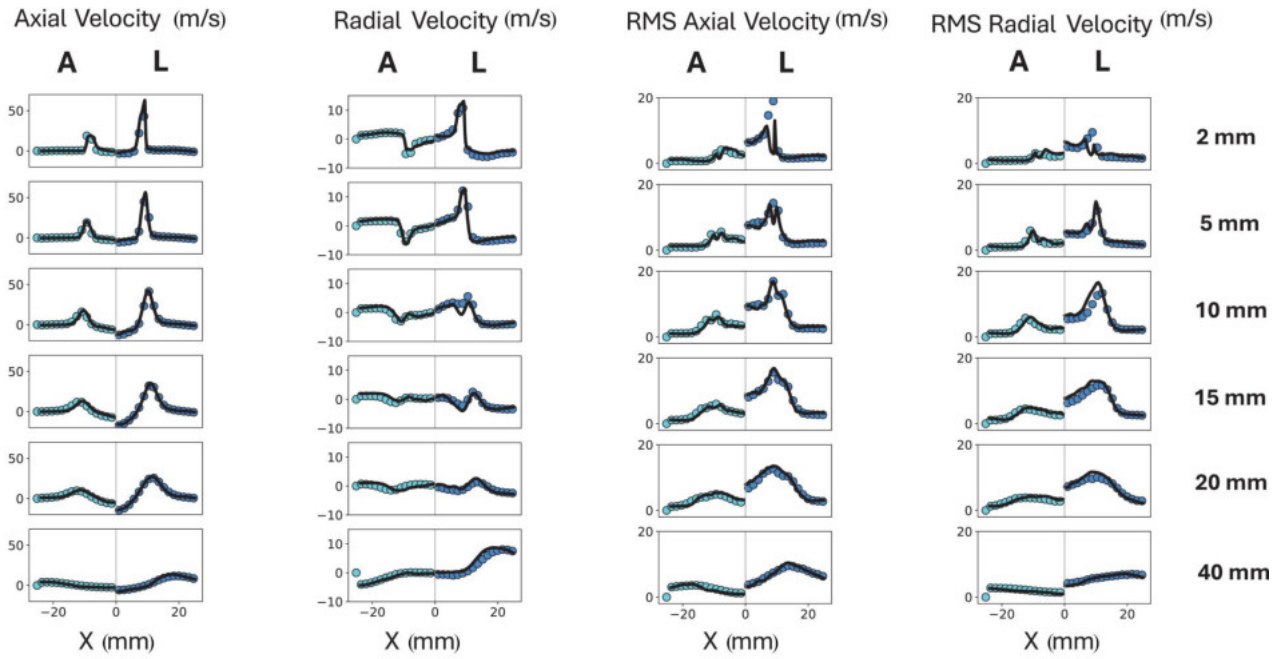

Fig. 14 HYLON cold flow simulation of both A (left) and L (right) configuration (LES:▬, Exp: circles)

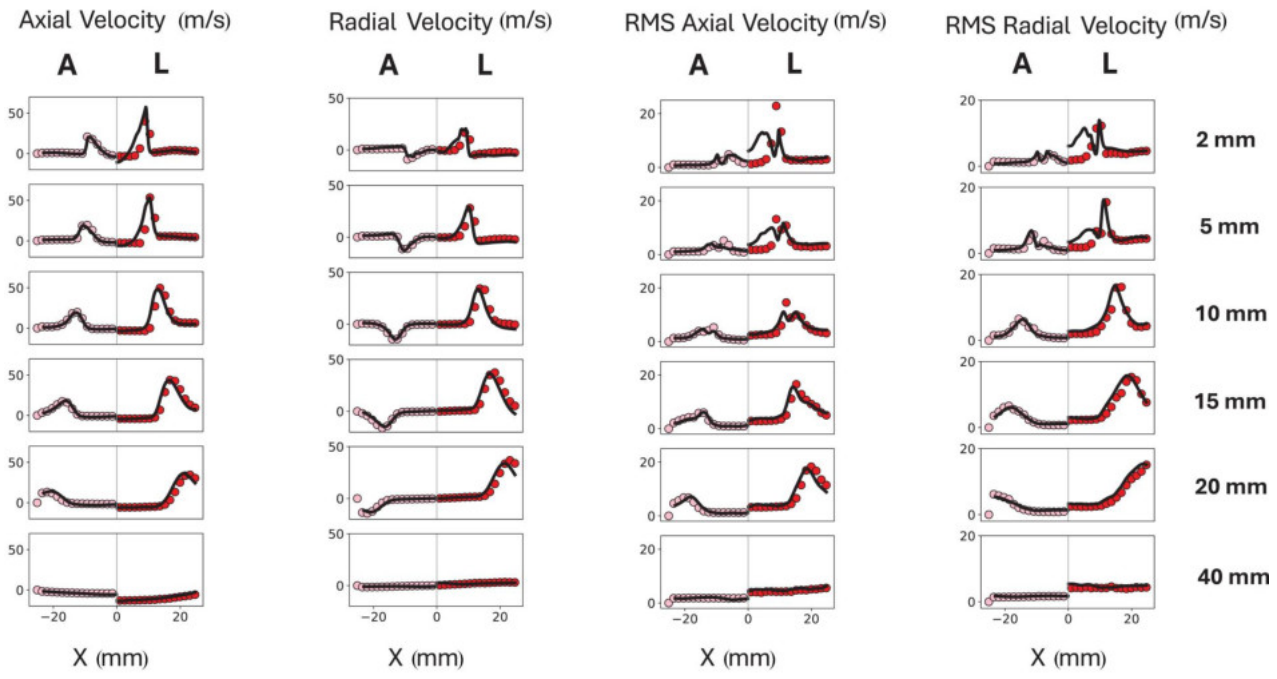

Fig. 15 HYLON reactive flow simulation of both A (left) and L (right) configuration (LES:▬, Exp: circles)

$$s_d = s_l^0 \left(\frac{\rho_u}{\rho_b}\right)^{1/2} \tag{6}$$

where s_l^0 is the maximum laminar flame speed and ρ_u/ρ_b is the volumetric expansion ratio of the gas through the flame for Z_0. The mixture fraction Z_0 in most cases is equal to Z_m associated with the maximum laminar burning velocity and maximum triple flame speed. These quantities have been calculated with Cantera [36] using a freely propagating hydrogen flame and the reduced GRI mech 3.0 (9 species 29 reactions).

Table 5 Mean temperature at the burner's exhaust for the HYLON test case

Flame	T_{exp} (K)	T_{TF} (Aniello et al.) (K)	T_{CFD} (K)
A	1138	1010 (−11%)	1338 (+17%)
L	1280	1100 (−16%)	1246 (−2.6%)

Mean temperature of gases at the outlet: T_{exp} indicates the temperature measured in the experiment; T_{CFD} are the results from the simulations performed in the present work; T_{TF} indicates the results obtained by Aniello et al. [14].

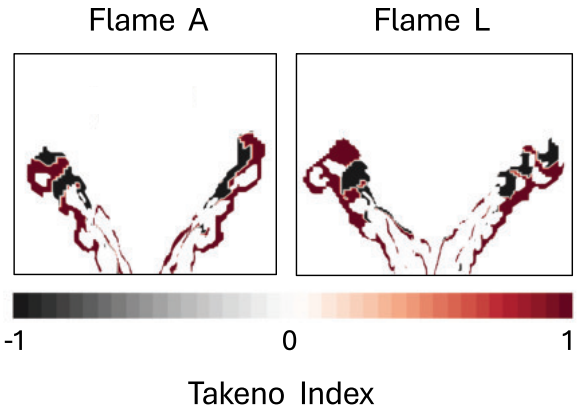

Fig. 16 Instantaneous contour plot of the Takeno Index for both the flames A (left) and L (right). A value of +1 indicates premixed combustion, while a value of −1 corresponds to nonpremixed combustion.

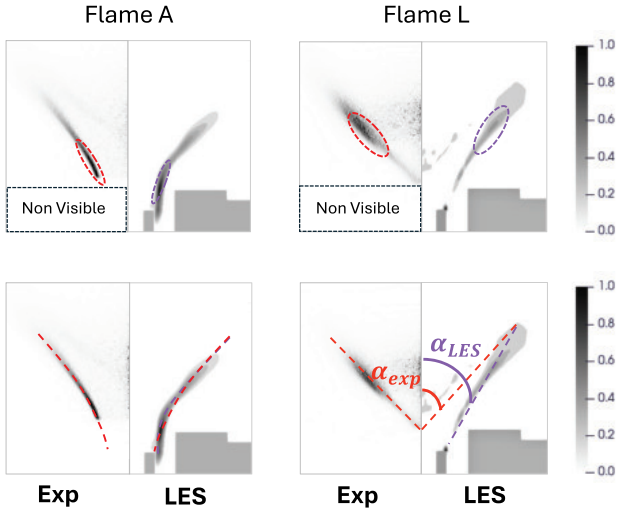

Fig. 17 Comparison between the experimental data (- - -) (left column) and the time-averaged OH* mass fraction (- - -) (right column). In the two figures at the top the zones with the largest release of energy due to combustion are highlighted. The figures below show a comparison of the opening angle of the flame α between the experimental data α_{exp} and numerical results α_{LES}.

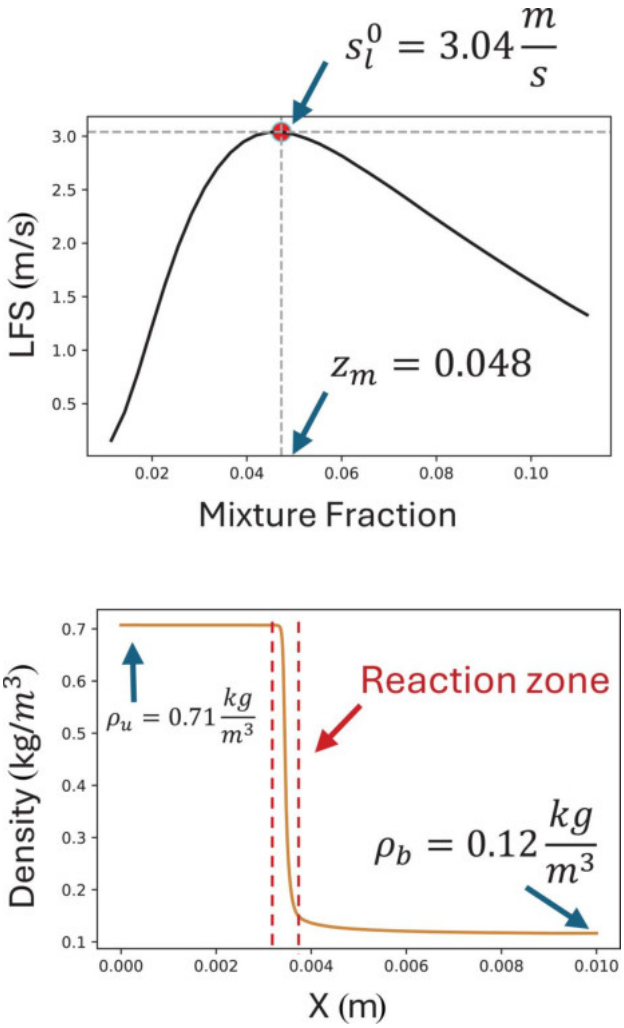

Fig. 18 Cantera simulations of the freely propagating premixed flames for the calculation of the s_d. The top figure on shows the calculation of the maximum burning laminar velocity s_l^0. The figure below shows the calculation of the volumetric expansion ρ_u/ρ_b of the gases due to the combustion process for a freely propagating premixed flame with a mixture fraction of Z_m.

First, the laminar flame speed was calculated for different compositions of the mixture to calculate the maximum laminar flame speed, obtaining a value of 3.14 m/s as shown in Fig. 18(*a*). From the value of maximum laminar flame speed and the mixture fraction at which this value occurs ($Z_m = 0.048$), another freely propagating flame at the mixture fraction Z_m was simulated to find the volumetric expansion ratio of the gas ρ_u/ρ_b, obtaining a value of 5.91 as highlighted in Fig. 18(*b*). The edge flame speed is at this point calculated and equal to 7.39 m/s. Once this value is determined, it becomes possible to verify whether the conditions for obtaining a lifted flame are satisfied. As shown in Fig. 19, the purple line, representing the isocontour of , intersects the TFUP region for Flame A but lies entirely outside the TFUP region for Flame L, in accordance with condition (ii) of the TFUP model. This calculation illustrates how the LES predictions align with experimental observations regarding the occurrence of an anchored or lifted flame.

5 Computational Cost

The simulations were conducted on a high-performance computing cluster using 8 × 32-core Intel Xeon Platinum 8358 (Ice Lake) CPUs. The computations were initially conducted using RANS

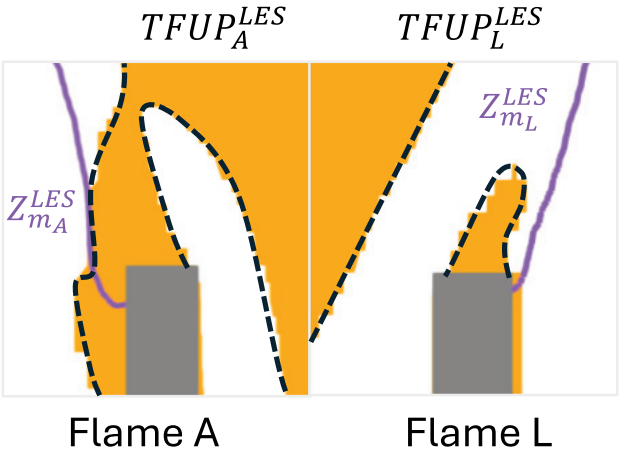

Fig. 19 TFUP model proposed by Marragou et al. [11]. The solid line (—) represents the isocontour of the mixture fraction at which the maximum laminar burning velocity occurs. The TFUP is colored in orange and represents the zone of the flow where the mean axial velocity is lower than the triple flame speed s_d.

simulations before transitioning to LES. Time-averaged data were collected over four flow-through times for each case, after the influence of the initial RANS solution was fully dissipated. The estimated computational cost was approximately 40,000 core hours for the NTNU case and 30,000 core hours for the HYLON case.

6 Summary and Conclusions

Premixed and nonpremixed hydrogen flames were investigated using LES and flamelet models with the main aim of assessing the capability of the simulations to predict the flame structure and characteristics of the reacting field in two different regimes. Numerical results show that the flamelet models are able to capture with good accuracy both the turbulent field and flame structure.

In the premixed configuration, results demonstrate that the LES-FGM approach provides a good prediction of the flow field measured in the experiment. The agreement between experimental and numerical data is better in the reactive case compared to the isothermal conditions. In addition, the model is able to capture the flame location and shape, although some discrepancies arise in the prediction of the thickness of the flame brush. As far as the nonpremixed flame is concerned, results show a better agreement with the experimental data compared to the premixed case. The model is able to predict the velocity field in both the nonreactive and reactive flow, with only some discrepancies in the prediction of the velocity fluctuations in the inner recirculation zone. The flamelet models used in these simulations are able to predict the shape of the flame and the peak location of the heat release rate. Considering the prediction of the flame shape, the simulation has turned out more accurate for the anchored configuration than for the lifted one. Conversely, the most accurate prediction of the averaged static temperature at the exhaust was obtained for the lifted flame. The outcomes of this study comprehensively validate LES and flamelet methods, contributing to more informed selection of numerical frameworks for industrial simulation scenarios.

Acknowledgment

This paper reflects only the authors' views and opinions; neither the European Union nor the European Commission can be considered responsible for them.

Funding Data

- Italian Ministry of University and Research under the Next-Generation EU Program (National Recovery and Resilience Plan–PNRR, M4C2, INVESTMENT 1.5–DD 1056 of 23/06/2022, ECS00000038, CUP F53C22000430001).

Data Availability Statement

The datasets generated and supporting the findings of this article are obtainable from the corresponding author upon reasonable request.

Nomenclature

Roman Letters

c = un-normalized progress variable
d = diameter (mm)
HRR = heat release rate (W m^{-3})
LHV = lower heating value (MJ/kg)
$\dot{m}$ = mass flow rate (kg/s)
p = pressure (Pa)
PFR = product formation rate (1/s)
T = temperature (K)
TFUP = triple flame upstream propagation
Z = mixture fraction

Greek Symbols

$\beta-$PDF = beta probability density function
μ = molecular dynamic viscosity (Pa s)
ρ = density [kg m^{-3}]
χ = scalar dissipation rate (s^{-1})

Dimensionless Groups

Pr = Prandtl number
Sc = Schmidt number
σ = Prandtl/Schmidt number

Superscripts and Subscripts

air = air stream
amb = ambient conditions
b = burnt mixture
H_2 = hydrogen stream
SGS = sub-grid scale property
t = turbulent property
u = unburnt mixture
$\sim$ = Favre filtered

Appendix A: Resolved Turbulent Kinetic Energy

A.1 Norwegian University of Science and Technology Case. The contour plot of the Cèlik criterium for the NTNU test case is shown in Fig. 20. Results are reported for an x-y plane passing through the axis of the bluff-body and for three planes orthogonal to the bluff-body's axis and located at different axial positions.

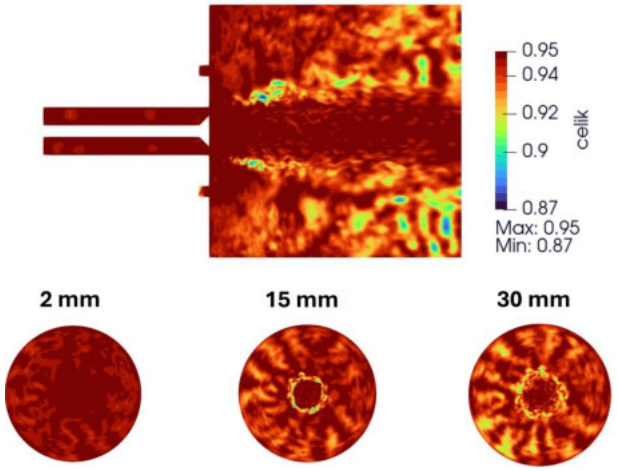

Fig. 20 Contour plot of the Celik criterium for LES quality in the reactive flow simulation for the NTNU test case

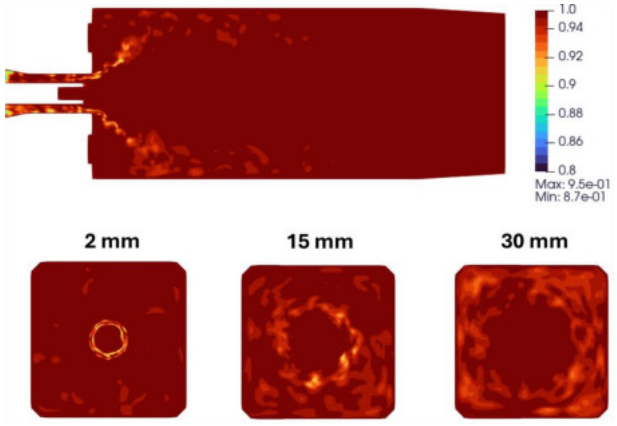

Fig. 21 HYLON contour plot of the Cèlik criterium for LES quality in the reactive flow of the anchored flame

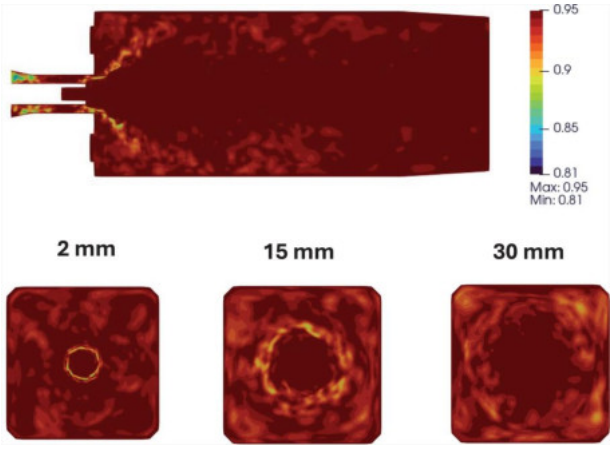

Fig. 22 HYLON contour plot of the Cèlik criterium for LES quality in the reactive flow of the lifted flame

A.2 HYdrogen LOw NOx Case. Figures 21 and 22 show the contour plots of the Cèlik criterium for flames A and L, respectively. Also in this case, the overall resolved turbulent kinetic energy is above 80%.

References

[1] Milton, B., and Keck, J. C., 1984, "Laminar Burning Velocities in Stoichiometric Hydrogen and Hydrogen-Hydrocarbon Gas Mixtures," Combust. Flame, **58**(1), pp. 13–22.

[2] Bouvet, N., Halter, F., Chauveau, C., and Yoon, Y., 2013, "On the Effective Lewis Number Formulations for Lean Hydrogen/Hydrocarbon/Air Mixture," Int. J. Hydrogen Energy, **38**(14), pp. 5949–5960.

[3] Sánchez, A. L., and Williams, F. A., 2014, "On the Effective Lewis Number Formulations for Lean Hydrogen/Hydrocarbon/Air Mixture," Prog. Energy Combust. Sci., **41**, pp. 1–55.

[4] Liu, W., Sun, L., Li, Z., Fujii, M., Geng, Y., Dong, L., and Fujita, T., 2020, "Trends and Future Challenges in Hydrogen Production and Storage Research," Environ. Sci. Pollut. Res., **27**(25), pp. 31092–31104.

[5] Mira, D., Lehmkuhl, O., Both, A., Stathopoulos, P., Tanneberger, T., Reichel, T. G., Paschereit, C. O., Vázquez, M., and Houzeaux, G., 2020, "Numerical Characterization of a Premixed Hydrogen Flame Under Conditions Close to Flashback," Flow Turbul. Combust., **104**(2–3), pp. 479–507.

[6] Ganguly, R., and Puri, I. K., 2004, "Nonpremixed Flame Control With Microjets," Exp. Fluids, **36**(4), pp. 635–641.

[7] Landry-Blais, A., Sivić, S., and Picard, M., 2022, "Micro-Mixing Combustion for Highly Recuperated Gas Turbines: Effects of Inlet Temperature and Fuel Composition on Combustion Stability and NOx Emissions," ASME J. Eng. Gas Turbines Power, **144**(9), p. 091014.

[8] McAllister, S., Chen, J.-Y., and Fernandez-Pello, A. C., 2011, *Fundamentals of Combustion Processes*, Springer, New York.

[9] Nemitallah, M. A., Abdelhafez, A. A., and Habib, M. A., 2020, *Approaches for Clean Combustion in Gas Turbines*, Springer, Cham, Switzerland.

[10] Gao, Y., Zhang, X., Han, W., Li, J., and Yang, L., 2022, "Effects of Swirl Number and Bluff Body on Swirling Flow Dynamics," AIP Adv., **13**(2), p. 25246.

[11] Marragou, S., Magnes, H., Aniello, A., Guiberti, T., Selle, L., Poinsot, T., and Schuller, T., 2023, "Modeling of H2/Air Flame Stabilization Regime Above Coaxial Dual Swirl Injectors," Combust. Flame, **255**, p. 112908.

[12] Æsøy, E., and Dawson, J. R., 2024, "Bluff Body Hydrogen Flame," NTNU, Trondheim, accessed Nov. 27, 2024, https://tnfworkshop.org/bluff-body-hydrogen-flame-ntnu-trondheim/

[13] Giusti, A., and Mastorakos, E., 2019, "Turbulent Combustion Modelling and Experiments: Recent Trends and Developments," Flow Turbul. Combust., **103**(4), pp. 847–869.

[14] Aniello, A., Laera, D., Marragou, S., Magnes, H., Selle, L., Schuller, T., and Poinsot, T., 2023, "Experimental and Numerical Investigation of Two Flame Stabilization Regimes Observed in a Dual Swirl H2-Air Coaxial Injector," Combust. Flame, **249**(4), p. 112595.

[15] Ballotti, A., Castellani, S., and Andreini, A., 2024, "A Dynamic Thickening Strategy for High-Fidelity Computational Fluid Dynamics Analyses of Multi-Regime Combustion," ASME J. Eng. Gas Turbines Power, **146**(12), p. 121010.

[16] Kutkan, H., Amato, A., Campa, G., Tay-Wo-Chong, L., and Æsøy, E., 2022, "LES of Turbulent Premixed CH4/H2/Air Flames With Stretch and Heat Loss for Flame Characteristics and Dynamics," ASME Paper No. GT2022-82397.

[17] Kutkan, H., Amato, A., Campa, G., Ghirardo, G., Tay Wo Chong, L., and Æsøy, E., 2022, "Modeling of Turbulent Premixed CH4/H2/Air Flames Including the Influence of Stretch and Heat Losses," ASME J. Eng. Gas Turbines Power, **144**(1), p. 011020.

[18] Amerighi, M., Senatori, G., Yahou, T., Schuller, T., Dawson, J. R., and Andreini, A., 2025, "Complete Dynamics From Ignition to Stabilization of a Lean Hydrogen Flame With Thickened Flame Model," ASME J. Eng. Gas Turbines Power, **147**(4), p. 041019.

[19] Yahou, T., Detomaso, N., Selle, L., Poinsot, T., Dawson, J., Schuller, T., and Laera, D., 2024, "The Role of Preferential Diffusion on the Ignition Dynamics of Lean Premixed Hydrogen Flames," Proc. Combust. Inst., **40**(1–4), p. 105612.

[20] Yahou, T., Dawson, J. R., and Schuller, T., 2023, "Impact of Chamber Back Pressure on the Ignition Dynamics of Hydrogen Enriched Premixed Flames," Proc. Combust. Inst., **39**(4), pp. 4641–4650.

[21] Æsøy, E., Aguilar, J. G., Bothien, M. R., Worth, N. A., and Dawson, J. R., 2021, "Acoustic-Convective Interference in Transfer Functions of Methane/Hydrogen and Pure Hydrogen Flames," ASME J. Eng. Gas Turbines Power, **143**(12), p. 121017.

[22] Æsøy, E., Nygård, H. T., Worth, N. A., and Dawson, J. R., 2022, "Tailoring the Gain and Phase of the Flame Transfer Function Through Targeted Convective-Acoustic Interference," Combust. Flame, **236**, p. 111813.

[23] Æsøy, E., Jankee, G. K., Yadala, S., Worth, N. A., and Dawson, J. R., 2023, "Suppression of Self-Excited Thermoacoustic Instabilities by Convective-Acoustic Interference," Proc. Combust. Inst., **39**(4), pp. 4611–4620.

[24] Massey, J. C., Langella, I., and Swaminathan, N., 2018, "Large Eddy Simulation of a Bluff Body Stabilised Premixed Flame Using Flamelets," Flow, Turbulence and Combustion, **101**(4), pp. 973–992.

[25] Ansys, 2023, "Fluent Theory Guide, Version R23.1," ANSYS Inc., Canonsburg, PA, accessed Aug. 25, 2025, https://ansyshelp.ansys.com/public/account/secured?returnurl=////Views/Secured/corp/v242/en/flu_th/flu_th.html

[26] Zimont, V., Polifke, W., Bettelini, M., and Weisenstein, W., 1997, "An Efficient Computational Model for Premixed Turbulent Combustion at High Reynolds Numbers Based on a Turbulent Flame Speed Closure," ASME Paper No. 97-GT-395.

[27] Smith, G. P., Golden, D. M., Frenklach, M., Moriarty, N. W., Eiteneer, B., Goldenberg, M., Bowman, C. T., et al., "Current and Future Releases of GRI-Mech," University of Berkeley, Berkeley, CA, accessed Aug. 25, 2025, http://www.me.berkeley.edu/gri_mech/

[28] Nori, V., and Seitzman, J., 2008, "Evaluation of Chemiluminescence as a Combustion Diagnostic Under Varying Operating Conditions," AIAA Paper No. 2008-953.

[29] Tyacke, J. C., and Tucker, P. G., 2015, "Future Use of Large Eddy Simulation in Aero-Engines," ASME J. Turbomach., **137**(8), p. 081005.

[30] Celik, I., Cehreli, Z., and Yavuz, I., 2005, "Index of Resolution Quality for Large Eddy Simulations," ASME J. Turbomach., **127**(5), pp. 949–958.

[31] Kai, R., Tokuoka, T., Nagao, J., Pillai, A. L., and Kurose, R., 2023, "LES Flamelet Modeling of Hydrogen Combustion Considering Preferential Diffusion Effect," Int. J. Hydrogen Energy, **48**(29), pp. 11086–11101.

[32] Klarmann, N., Sattelmayer, T., Geng, W., and Magni, F., 2016, "Flamelet Generated Manifolds for Partially Premixed, Highly Stretched and Non-Adiabatic Combustion in Gas Turbines," AIAA Paper No. 2016-2120.

[33] Yamashita, H., Shimada, M., and Takeno, T., 1996, "A Numerical Study on Flame Stability at the Transition Point of Jet Diffusion Flames," Symposium (International) ON Combustion, **26**(1), pp. 27–34.

[34] Knudsen, E., and Pitsch, H., 2012, "Capabilities and Limitations of Multi-Regime Flamelet Combustion Models," Combust. Flame, **159**(1), pp. 242–264.

[35] Luo, Y., Steinhausen, M., Kaddar, D., Hasse, C., and Ferraro, F., 2023, "Assessment of Flamelet Manifolds for Turbulent Flame-Wall Interactions in Large-Eddy Simulations," Combust. Flame, **255**, p. 112923.

[36] Goodwin, D. G., Moffat, H. K., Schoegl, I., Speth, R. L., and Weber, B. W., 2023, "Cantera: An Object-Oriented Software Toolkit for Chemical Kinetics, Thermodynamics, and Transport Processes," Zenodo, Geneva, Switzerland, accessed Aug. 25, 2025, https://www.cantera.org.